Determination of the spatial and temporal variation of tropospheric water vapour using CGPS networks

Author(s):
Troller, M.; Geiger, A.; Brockmann, E.; Kahle, H.-G.

Publication date:
2006-11

Permanent link:
https://doi.org/10.3929/ethz-b-000016834

Originally published in:
Geophysical Journal International 167(2), https://doi.org/10.1111/j.1365-246X.2006.03101.x

Geophys. J. Int. (2006) **167,** 509–520 doi: 10.1111/j.1365-246X.2006.03101.x

Determination of the spatial and temporal variation of tropospheric water vapour using CGPS networks

M. Troller,[1] A. Geiger,[1] E. Brockmann[2] and H.-G. Kahle[1]

[1] *Geodesy and Geodynamics Lab, Institute of Geodesy and Photogrammetry, ETH Zurich,* 8093 *Zurich, Switzerland. E-mail: troller@geod.baug.ethz.ch*
[2] *Swiss Federal Office of Topography, Geodetic bases and permanent networks, Wabern, Switzerland*

Accepted 2006 June 19. Received 2006 February 24; in original form 2004 December 6

SUMMARY

Tropospheric water vapour is the main limiting factor in using GPS to determine crustal deformation at highest accuracy. On the other hand, it is an important variable to monitor meteorological and climatic processes. This paper discusses both aspects: the modelling of tropospheric water vapour using meteorological data as well as the determination of the integrated amount of water vapour and its spatiotemporal variation using GPS data. Switzerland has been chosen as experiment area. The Swiss continuous GPS (CGPS) network AGNES is used as a reference network, which represents a realistic scenario for GPS-based water vapour determination. Data of the Swiss numerical weather model aLMo are used for systematic comparison and validation.

For the first aspect, integrated tropospheric wet refractivity values are determined from meteorological measurements and compared with GPS path delays. An overall agreement of 1 cm of zenith wet path delay was achieved. For the second aspect a tomographic approach has been developed. A total of 6720 GPS-determined profiles are compared with data of the numerical weather model and radio soundings. The results are statistically evaluated and systematically compared with each other. A correlation between the accuracy and the weather situation was found. Overall, an agreement of 5–7 ppm (refractivity unit) was obtained compared to aLMo.

The use of GPS-determined path delays from a permanent GPS network is the recommended method to correct GPS measurements. In all other cases, the two methods presented (COITROPA, COMEDIE) are a feasible alternative to determine path delays accurately. Furthermore, GPS is a convenient application to determine the amount of water vapour in the troposphere. It is demonstrated that the vertical distribution of water vapour can be deduced by applying the tomographic approach.

Key words: climate, GPS, satellite geodesy, tomography.

1 INTRODUCTION

Climate change has become of major concern for the future, facing the planet's environment and its population. In this context, water vapour plays a crucial role. It is the most variable parameter of the major constituents of the atmosphere, both in space and time. It is involved in many processes and chemical reactions such as the greenhouse effect, the decomposition of the ozone layer, the distribution of air pollution and acid rain.

The tropospheric water vapour causes a delay in the arrival of microwave signals propagating through the atmosphere. This effect is one of the main limiting factors and has to be corrected for accurate GPS positioning.

On the other hand, the total amount of water vapour in the atmosphere can be successfully determined using satellite navigation systems such as GPS (e.g. Bevis *et al.* 1992). To account for the 4-D distribution of water vapour in the atmosphere, a new technique called GPS tomography is under investigation (e.g. Troller *et al.* 2002). It is applied to an operational dense permanent GPS network. Accuracies of the total amount of water vapour and its spatial and temporal distribution are discussed.

The next generation of numerical weather prediction models requires precise 3-D information of the water vapour distribution with a high temporal resolution. In regions with a high density GPS network—such as the Swiss AGNES network—GPS can be an important data source for the numerical weather prediction.

2 AREA OF INVESTIGATION AND DATA SOURCES

Switzerland has been chosen as area of investigation. It is specially suited because of the topographic varieties from flat to mountainous alpine areas. Moreover, the Swiss National GPS permanent

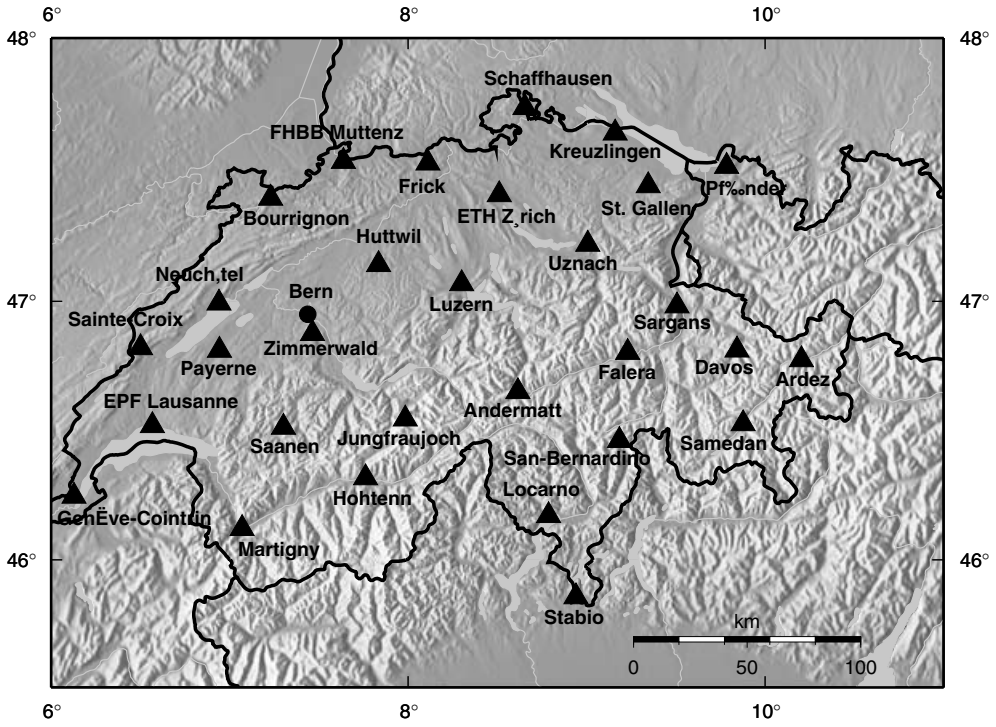

Figure 1. GPS stations of the AGNES network in Switzerland operated by the Swiss Federal Office of Topography. The automated AGNES processing includes the AGNES stations (triangles) as well as 20 EUREF stations and 23 stations from other networks (circle). The figure shows the stations in Switzerland only.

network AGNES (Automated GPS NEtwork of Switzerland) provides high-density data sets (Fig. 1). AGNES consists of 30 stations, equally distributed over the entire Swiss territory. The altitudes range from 329 to 3584 m. The data of all AGNES stations are automatically processed at the Swiss Federal Office of Topography using the Bernese GPS Software (Beutler *et al.* 2001). Additionally, the data of 20 EUREF stations are used to enlarge the station network to achieve accurate results (Brockmann & Troller 2002). Means of zenith total delays are provided on an hourly basis.

Meteorological ground data of air pressure, temperature and humidity are provided by the Automated Meteorological Network ANETZ of the Swiss Meteorological Office. Hourly means of pressure and ten-minutes-values of temperature and humidity are available at 72 ground stations. The data are complemented with radiosonde data of the Swiss radiosonde station Payerne and further stations in the neighbourhood. Radiosondes are launched usually twice a day, sometimes four times a day.

Furthermore, data of the operational, high resolution numerical weather model aLMo (aLpine Model) of MeteoSwiss are used. aLMo is the Swiss implementation of the non-hydrostatic local weather model called COSMO (COnsortium of SMall-scale MOdelling) (Doms & Schättler 2003). aLMo consists of 385 × 325 grid points with a horizontal grid spacing of around 7 km. Forty-five levels are used in the vertical. Two 72 hr forecasts are calculated daily, however, for the investigations in this study, only the data of the assimilation cycles are used which represent the best possible state of the atmosphere as viewed by aLMo.

The days of 2002 November 3–9, have been used as investigation period because rapid weather changes occurred during this period. After heavy rainfall in the morning of November 3, bright intervals interrupted the rainfall in the afternoon. During the next two days, wet air reached Switzerland continuously and caused further rainfall. Only the southern part of Switzerland was sunny. On November 6, continental dry air predominated and lead to a sunny day in the whole country. On the next day, wet air arrived and caused rainfall in the afternoon in the northern part of Switzerland. A belt of high pressure allowed sunshine on November 8 and in the morning of November 9. Further rainfall occurred on the same afternoon.

3 ZENITH WET PATH DELAYS

The determination of zenith wet path delays is important, both to correct for the tropospheric error in GPS measurements and to monitor the variation of the total water vapour amount in the troposphere on a continuous basis.

In the first part of this study, five different ways of determining zenith wet path delays have been analysed:

Saastamoinen: The classical approach of determining path delays is to use standard models like Saastamoinen (1972) which are parametrized by ground meteorological data only. Usually, such an approach works well if standard atmospheric conditions apply: exponential decrease of pressure and water vapour pressure with altitude and a linear decrease of temperature with altitude up to the tropopause.

COMEDIE: The state of the atmosphere (pressure, temperature, water vapour pressure) is modelled in space and time using a collocation approach. The software package COMEDIE (COllocation of MEteorological Data for Interpolation and Estimation of tropospheric path delays) was developed at our institute. It allows to process any spatially and temporally distributed meteorological measurements (see Appendix A, e.g. Troller *et al.* 2000; Troller 2004). In the subsequent evaluations, ground meteorological data of the ANETZ network are introduced and radiosonde data of several launches in and around Switzerland. Path delays along arbitrary

ray paths are obtained by integrating the collocated refractivity on the path.

aLMo: Vertical profiles of meteorological data are available from numerical weather models such as aLMo. Wet path delays can be determined by integrating the refractivity along the profile.

AGNES: Zenith path delays can be determined with high accuracy by GPS (Beutler *et al.* 2001) at the stations of the continuous GPS network AGNES.

COITROPA: With the increasing number of permanent GPS stations in the recent years, a new approach to model the path delay has become applicable. GPS-derived zenith path delays are used as input data, to interpolate zenith path delays spatially and temporally. The software package COITROPA (COllocation and Interpolation of TROpospheric PAth delays) was developed. Similar to COMEDIE, COITROPA is based on a 4-D collocation in space and time (see Appendix B, e.g. Troller 2004).

Comparisons of the different zenith path delay determinations are performed at the locations of the 30 AGNES stations during 1 week. A generally good agreement of the various methods was reached at all AGNES stations during the investigation period. The plots of the stations STGA (St. Gallen) and DAVO (Davos) are given in Fig. 2. STGA is located in the Swiss pre-alpine area (altitude 754 m), DAVO in the alpine area (altitude 1646 m). It is clearly seen that the wet path delays are strongly dependent on the weather situation. The interruption of heavy rainfall on November 3, lead to a rapid decrease of the wet path delay. Further rainfall on November 7 and 9 caused a new increase of wet path delay at these respective time periods.

The excellent fit of the COITROPA solution with GPS-derived data (AGNES) within 1 cm is clearly visible. The data of the numerical weather model aLMo fits almost equally well. Also the COMEDIE solution fits to the AGNES data. However, COMEDIE is unable to reproduce short-time variations. This can be attributed to the simplified functional models. The Saastamoinen solution shows large discrepancies on November 3, 6 and 9. These discrepancies appear because the Saastamoinen model is a relatively simple model in which a standard atmosphere is used based on ground meteorological measurements.

Furthermore, it has to be considered that the same data source is used to determine the AGNES and COITROPA solutions. The other three solutions stem from another (at least partially the same) data origin. Measurement errors are present and influence the statistical comparisons as well.

The deviations of all data series with respect to the AGNES solution are statistically evaluated. Fig. 3 shows the rms values of the deviations at the AGNES stations versus altitude. COITROPA fits

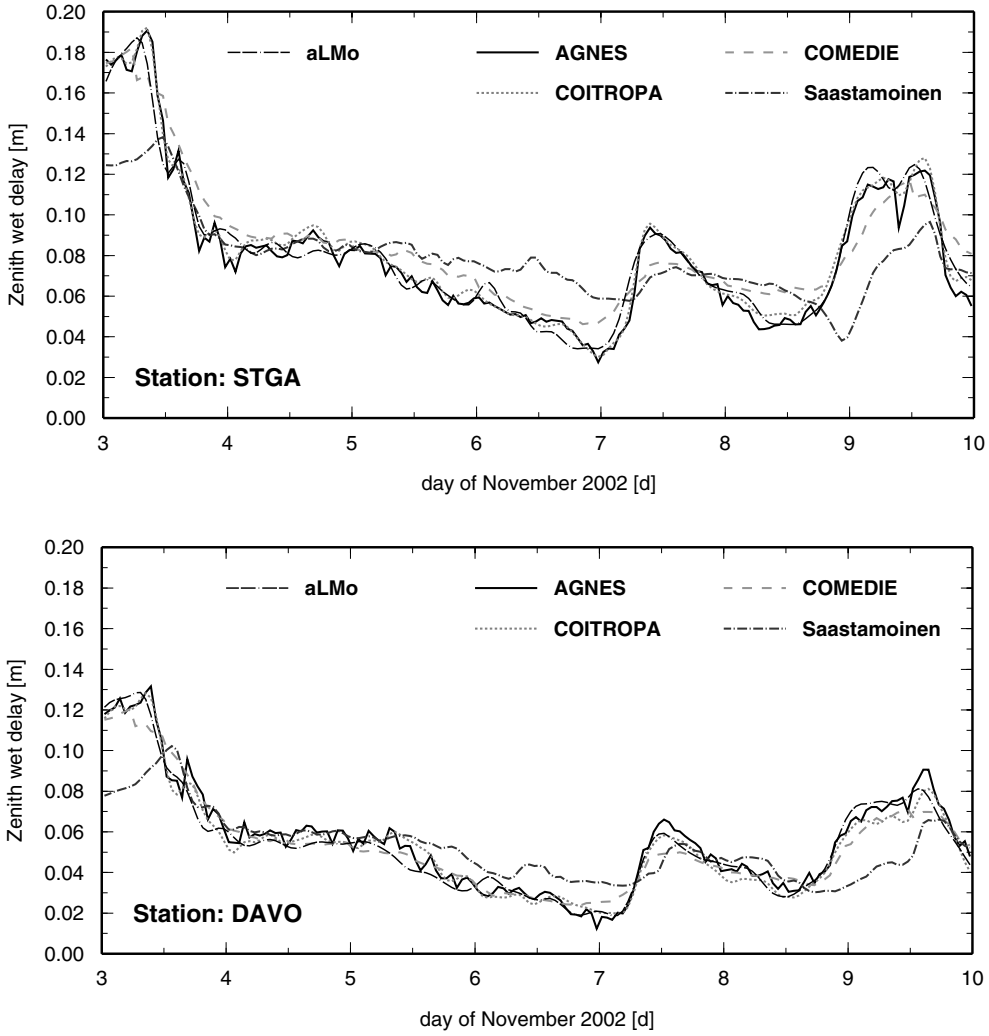

Figure 2. Zenith wet delay at AGNES station STGA and DAVO. The plot at STGA represents a typical situation for a station in the for-alpine area, DAVO in the alpine area.

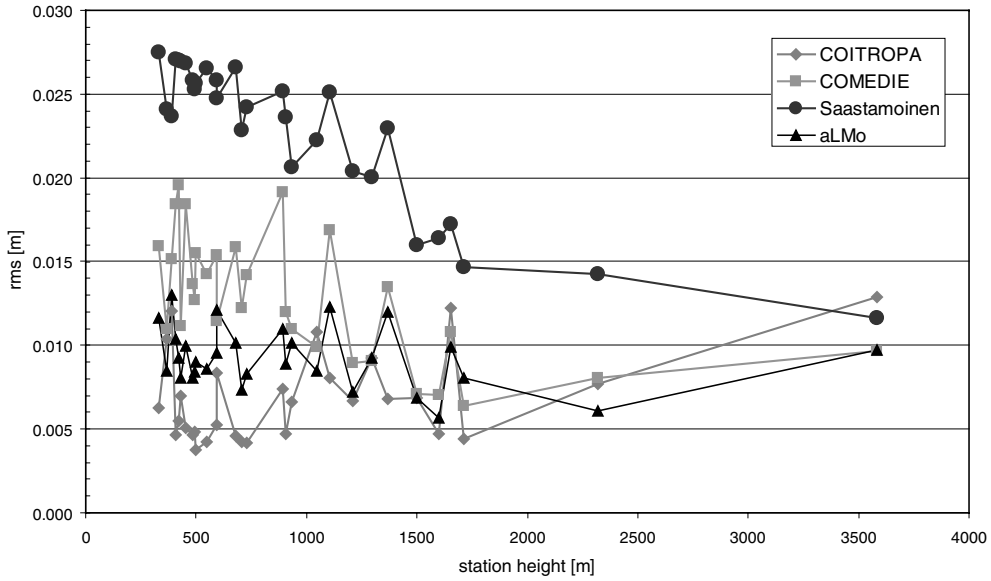

Figure 3. Statistical evaluation of COITROPA, aLMo, COMEDIE and Saastamoinen with respect to AGNES. The plot shows the rms vs. station height. While the rms values stay approximately constant in the COITROPA and aLMo solutions, COMEDIE and specially the Saastamoinen solution become less accurate with decreasing altitude.

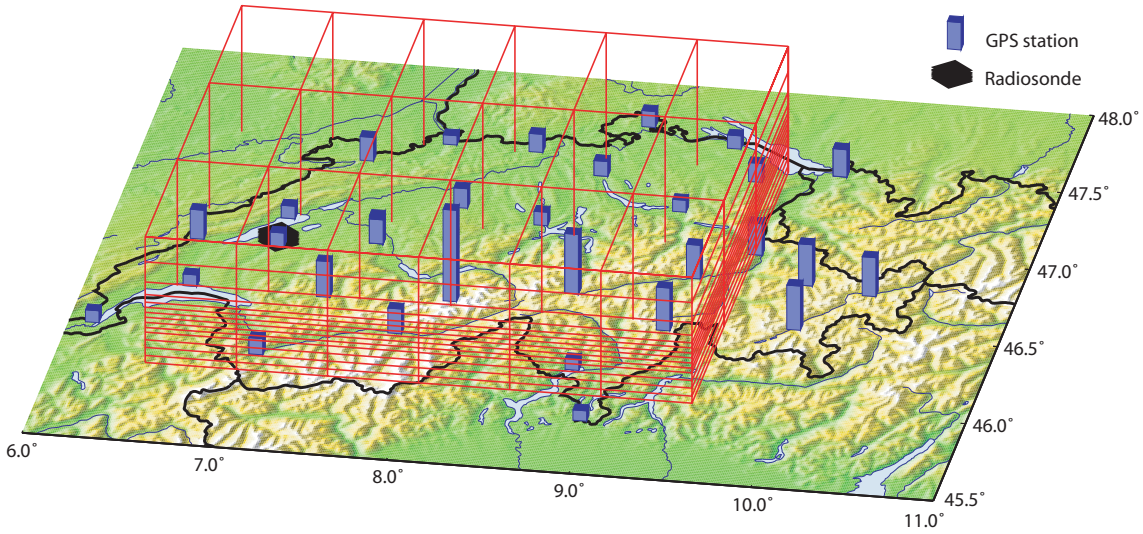

Figure 4. 3-D view of the tomographic voxel model above the Swiss territory. The figure shows the core voxel model of 6 × 3 voxels per layer, and layers up to 5000 m altitude. The open voxels, added at the horizontal boundaries of each layer, as well as the two uppermost layers (5000–8000 m, 8000–15 000 m) are not shown. The GPS stations of the AGNES network are shown as prisms (length of prism according to their station altitude). Radiosondes are launched at the station Payerne.

the AGNES data most accurately with a mean rms of 7 mm. A correlation of the COITROPA solution with the altitude is not seen. To obtain accurate COITROPA data, it is primarily necessary to have a regular GPS network for the interpolation.

The rms of the aLMo solution is independent of the altitude as well. A mean rms of 9 mm was reached in this study. Keeping in mind that the aLMo data are interpolated from a regular grid, the rms consists of the error of the original aLMo model and the error of the interpolation. The rms of the COMEDIE solution shows a small decrease with the altitude. A mean rms of 13 mm was reached. This can be attributed to the simplified modelling of the temperature and the water vapour pressure. The Saastamoinen solution has a mean rms of 23 mm. A decrease of the rms with altitude is clearly seen. This effect correlates with the decrease of the total amount of wet path delay with altitude.

4 WATER VAPOUR PROFILES

4.1 Method of GPS tomography

To resolve the spatial structure of the water vapour distribution in the atmosphere, the method of tomography is applied. The atmosphere is divided into a 3-D voxel model, each voxel i with a constant refractivity N_i. Ellipsoidal boundary surfaces of the layers account for the Earth's curvature. The wet slant path delay Δ_{wet}^{PD} of the

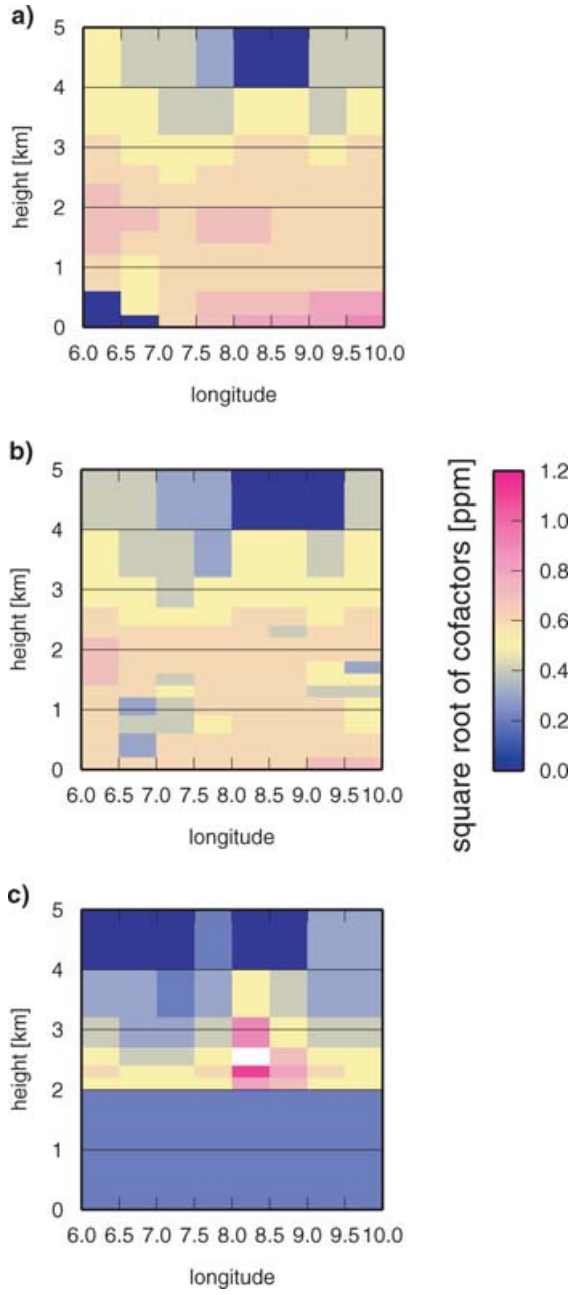

Figure 5. Cross section of the square root of cofactors at latitude 46.75°. The two top layers are not shown on the plots. (a) represents the solution AWATOS correlation, (b) AWATOS AGNES and (c) AWATOS ANETZ. If *a priori* refractivity is introduced, the accuracy is locally increased significantly.

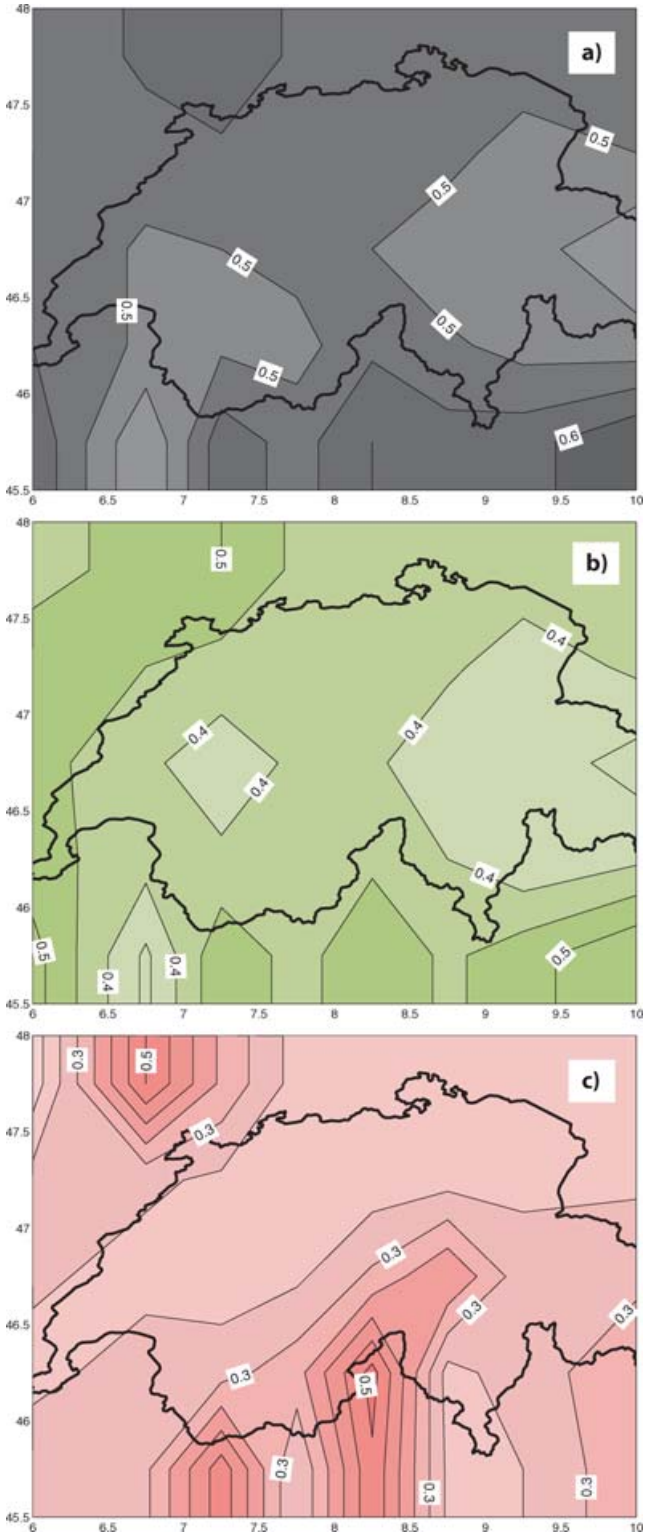

Figure 6. The contour map shows the *a priori* precision of the three solutions in ppm (refractivity unit, interval 0.05 ppm). (a) represents the solution AWATOS correlation, (b) AWATOS AGNES and (c) AWATOS ANETZ.

microwave signal from the GPS satellite to the receiver is discretized following the voxel model.

$$\Delta_{\text{wet}}^{PD} = 10^{-6} \cdot \int_{\text{receiver}}^{\text{satellite}} N\, ds = 10^{-6} \cdot \sum_i N_i \Delta s_i, \qquad (1)$$

Δs_i represents the length of the ray in voxel i. The ray bending effect can be ignored, as an elevation cut-off angle of 10 degrees is applied (Mendes 1999).

A tomographic software package called AWATOS (Atmospheric WAter vapour TOmography Software) has been developed (Kruse 2001; Troller *et al.* 2002). In the current approach, the main type of observations are GPS double-difference path delays from the GPS processing (Troller 2004). Thus, the satellite and receiver clock errors are pre-eliminated. A detailed description of the double-difference approach is given in Appendix C.

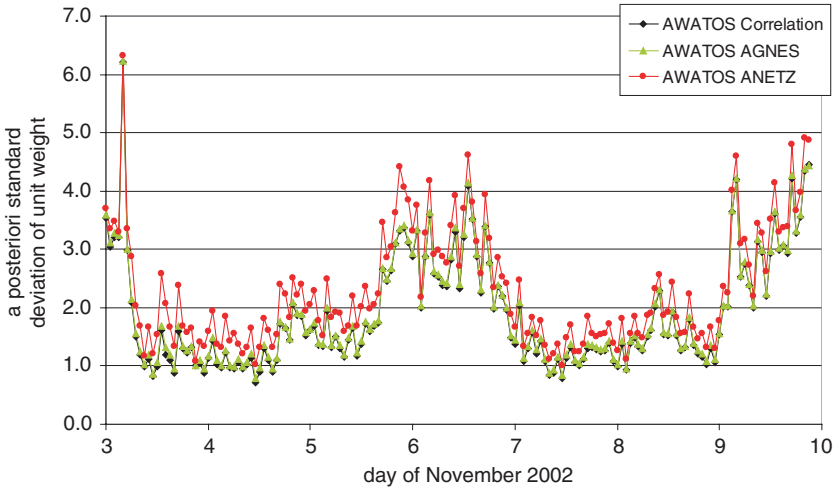

Figure 7. *A posteriori* standard deviation of unit weight of the tomographic solutions during the investigation period.

The number of traversing rays per voxel depends on the geometry defined by the distribution of the ground GPS stations as well as the satellite constellation and on the resolution of the voxel model. Usually, only a part of the voxel refractivities are sufficiently determined and the other part is underdetermined. The whole equation system is mixed-determined (Menke 1989), and the inversion may become singular.

The singular value decomposition (SVD) is able to diagnose and separate the underdetermined part in a way, that the overdetermined part of the equation system can be solved (Press *et al.* 1994). However, simulations show that the solution of the overdetermined part still remains very weak, yielding an unacceptable low accuracy (Troller 2004).

In the following, additional voxel constraints (pseudo-observations) are used to stabilize the system of equations. Two types of constraints are applied:

(i) Refractivity information obtained from independent sources can be used to constrain certain voxels. It is generally accepted, that the amount of water vapour is nearly zero above 5000 m altitude. Therefore, this *a priori* information is used to constrain the uppermost voxel layer. Furthermore, ground meteorological measurements can provide *a priori* information.

(ii) Voxels are mutually coupled to limit the variation in refractivity of neighbouring voxels (intervoxel constraints). The weighting of the individual neighbouring voxels is derived from a covariance function. To allow steep refractivity gradients, only direct neighbouring voxels are correlated (see Appendix D for a detailed description).

4.2 Experimental set-up and *a priori* analysis

A voxel model above the Swiss territory was designed according to the station density of the GPS network. It consists of 6×3 core voxels in the horizontal dimension and 16 layers up to 15 000 m. The thickness of the layers vary from 300 m in the lower troposphere to several thousand metres in the stratosphere (Fig. 4). At the horizontal boundaries in each layer, open voxels are added, which reach ad infinitum. Thus, all the rays do pass completely inside the model.

The following evaluation contains three solutions, differing in the use of the constraints (the ideal weighting of the constraints for each solution has been determined heuristically):

AWATOS correlation: The solution contains intervoxel constraints between all voxels. The constraints are down-weighted compared to the double-difference observations by a factor of 50^2 (regularization factor $= \frac{1}{2500}$).

AWATOS AGNES: In addition to the intervoxel constraints, AWATOS AGNES contains *a priori* refractivity data, measured at each location of the AGNES station. This solution is based on the concept, that only a small additional effort is necessary to perform meteorological measurements at GPS stations. Like the intervoxel constraints, the *a priori* meteorological constraints are down-weighted by a factor of 50^2 compared to the observations.

AWATOS ANETZ: In this solution, one *a priori* refractivity value for each voxel lower than 2000 m is introduced. The refractivity values are interpolated using the ANETZ data and COMEDIE. The border value of 2000 m has been chosen, as COMEDIE is usually able to interpolate ANETZ data sufficiently accurately up to this altitude. These constraints are down-weighted by a factor of 20^2 (regularization factor $\frac{1}{400}$).

The *a priori* quality of the three solutions can be investigated by evaluating the cofactor matrices, assessing the geometry and the weighting of the measurements only. No measurements are taken into account. The use of intervoxel constraints only (AWATOS correlation), leads to a profile with a precision increasing with height (Fig. 5). The introduction of *a priori* refractivity values increases the precision of the respective voxel significantly. The voxels with *a priori* refractivity in Fig. 5 are evident. Furthermore, the whole equation system is strengthened and the precision of the whole voxel model is increased.

To evaluate the *a priori* quality of the three solutions in the investigation area, the precision of each profile has been calculated by averaging the square root of the cofactor values of the associated voxels. Due to the high density GPS network, no significant precision difference is visible in different parts of Switzerland (Fig. 6). However, the precision in the alpine area is usually somewhat lower. The solution AWATOS ANETZ has a significantly smaller precision outside of Switzerland because of missing ANETZ stations.

4.3 Data analysis and error budget

The GPS measurements are prepared along with the *a priori* refractivity values calculated, for the tomographic adjustment of the

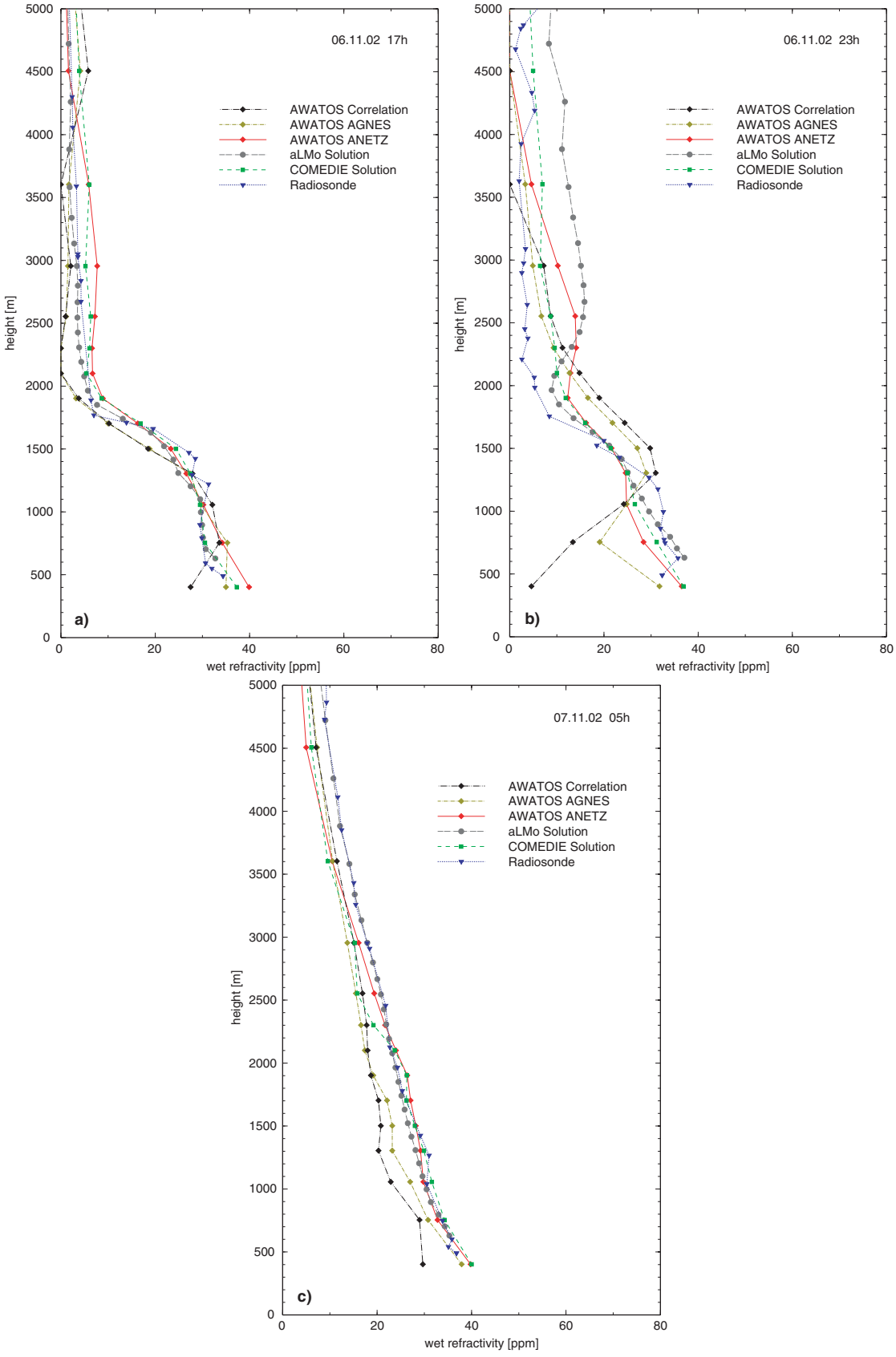

Figure 8. Wet refractivity profiles of three different tomographic solutions (AWATOS correlation, AWATOS AGNES, AWATOS ANETZ), a solution using COMEDIE, a refractivity profile obtained by a radiosonde launch at station Payerne and data of the numerical weather model aLMo. Panel (a) shows a profile with a rapid refractivity change at 1800 m altitude. Panel (b) shows an irregular decrease of the refractivity with height. Panel (c) shows a profile with a more linear decrease of the refractivity in height.

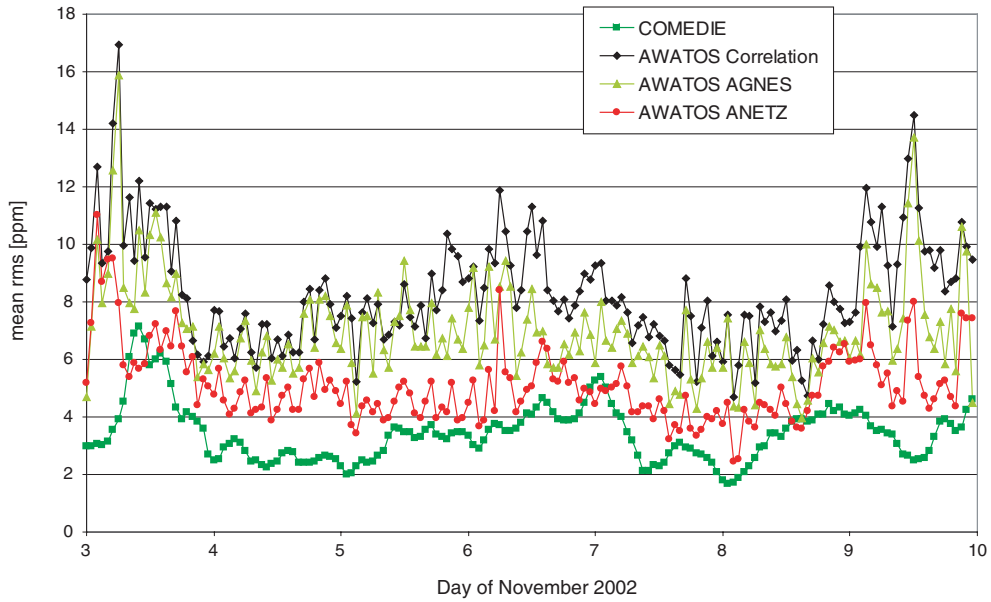

Figure 9. Time-series of the mean rms of all profiles compared to aLMo. Overall, the COMEDIE solution has the smallest rms, followed by the solution AWATOS ANETZ.

equation system. The refractivity of each voxel is determined by 1 hr data assimilation. From each vertical column of the voxel model, a vertical refractivity profile can be drawn. For a 1 week period at a 1 hr resolution, 6720 vertical profiles can be extracted for quality assessment. To inspect the precision of the hourly tomographic determination, the *a posteriori* standard deviation of unit weight was calculated (Fig. 7). A strong variation is visible. The highest values are present on November 3, 6 and 9. It is assumed, that the state of the atmosphere influences the precision.

The *a posteriori* standard deviation of each refractivity value and subsequently each profile (mean of a refractivity column) is calculated. Finally, the mean *a posteriori* standard deviations of all profiles are determined. Values around 0.8 ppm (refractivity unit) resulted for the AWATOS correlation and AWATOS AGNES solution and 0.6 ppm for the AWATOS ANETZ solution. The precision for the core profiles is marginally higher than for the border profiles.

4.4 Profile evaluation and statistical comparison

The refractivity profiles of the tomographic solutions are compared with independently generated profiles from:

aLMo Solution: Hourly profiles of the aLMo model of MeteoSwiss are directly used for comparison.

COMEDIE Solution: Using the ANETZ data and radiosondes, COMEDIE allows to estimate the wet refractivity for each voxel. The values are calculated with a sampling rate of 1 hr.

Radiosonde: Radiosondes are launched usually twice or four times a day from the radiosonde station Payerne. A total of 22 launches have been carried out during the time of investigation.

The aLMo solution has been taken as reference for a statistical analysis. For each profile, the deviations of the associated voxels to aLMo have been evaluated. The degree of agreement of the individual profiles varies. The revealed rms are in the range of 5–10 ppm with a few outliers reaching 20 ppm.

Fig. 8(c) shows a profile with a smooth decrease of the refractivity as a function of the height. All solutions match the aLMo solution. An rms between 2.5 ppm (refractivity unit) for the solution AWATOS ANETZ to 5.7 ppm (AWATOS correlation) is achieved. Profile (a) reveals a rapid refractivity change at around 1800 m altitude. This behaviour cannot easily be represented by a covariance function and, therefore, the reproduction requires reliable GPS measurements. This holds true, in particular for the solution AWATOS correlation that contains only double-difference observations and a covariance function. All solutions fit the numerical weather model determination well; an rms of 2.3 (AWATOS ANETZ) up to 3.4 ppm (AWATOS correlation) was obtained. GPS tomography has the potential to estimate the 3-D water vapour refractivity in the atmosphere. However, in profile (b), particularly the wet refractivity of the solution AWATOS correlation is underestimated below an altitude of 1000 m. The rms increases to 4.9 ppm (AWATOS ANETZ) and to 9.2 ppm (AWATOS correlation), respectively.

The COMEDIE solution is not independent from the aLMo solution. In part, the same input data is introduced in both models. However, in the higher troposphere, COMEDIE follows a standard atmosphere model. If temperature inversions or other irregularities are present, an offset to aLMo appears. The radiosonde profiles, whose data are assimilated to the weather model as well, fit accurately to aLMo most of the time on the order of 2–3 ppm. Rarely, rapid refractivity changes that are recorded by the radiosondes are not reproduced by aLMo.

Fig. 9 shows the mean rms of all profiles at a specific time point during the investigation. It is clearly seen, that the rms of the solution AWATOS ANETZ is generally smaller than that of the other solutions. However, a correlation between the different tomographic solutions is obvious and three outlier regions are found. Comparing with the prevailing weather situation, the outlier in the morning of November 3 can be explained with the humidity change due to heavy rain in the morning and bright intervals in the afternoon. The outlier period of November 6 corresponds to a rapid decrease of humidity. Finally, the outlier of November 9 in the morning coincides with the change from sunny weather in the morning to rain in the afternoon. In contrast to the tomographic solutions, the rms of the COMEDIE time-series does not show the same behaviour or the same outliers.

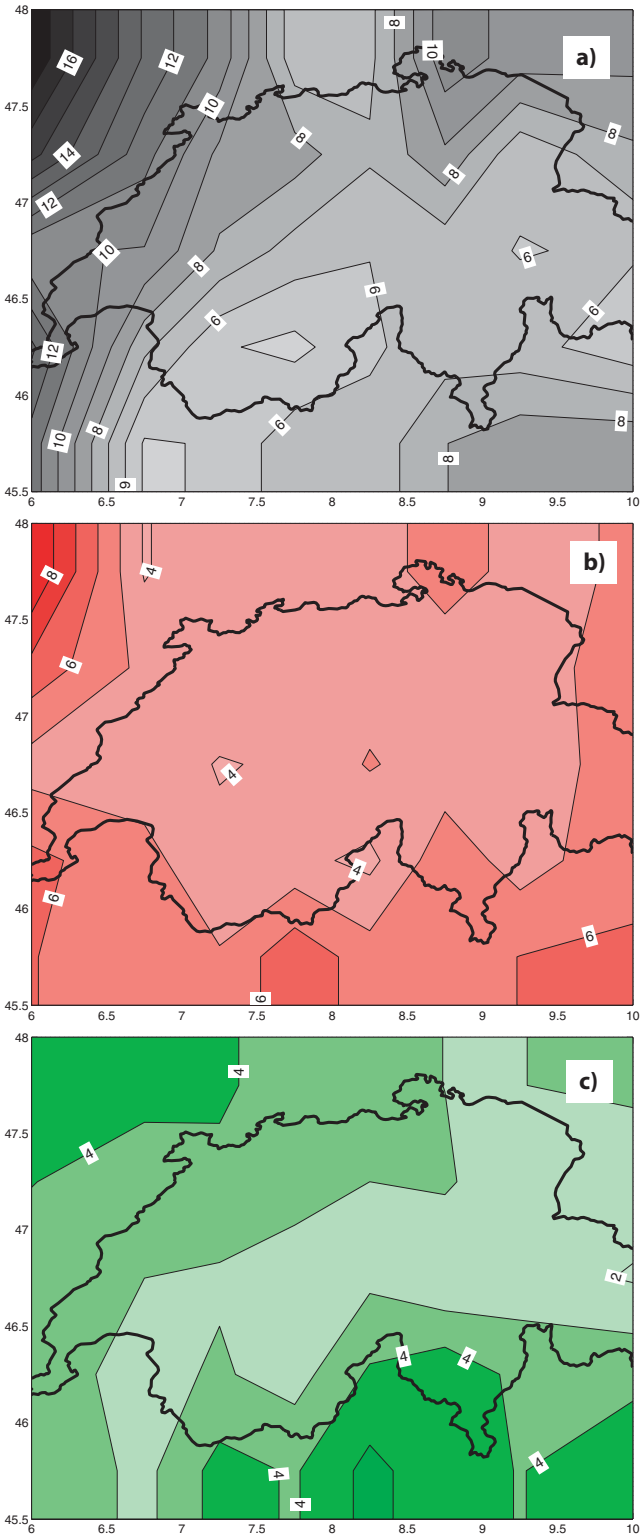

Figure 10. Mean of the profile rms of AWATOS correlation (a), AWATOS ANETZ (b) and COMEDIE (c) compared to aLMo. The figure shows contour maps with an interval of 1 ppm (refractivity unit), whereas each second interval is labelled.

Table 1. Correlation of stochastic parameters and variances for the collocation of pressure p, temperature T and water vapour pressure e. The variability of water vapour with height has to be taken into account with the choice of smaller correlation lengths in spatial as well as in temporal dimension. Abbreviations: σ_0: *a priori* standard deviation of the signal; σ_0(noise): *a priori* standard deviation of the noise; Δx_0, Δy_0, Δz_0, Δt_0: correlation length of the individual components; z_0: scaling height.

	σ_0 [hPa] or [°C]	Δx_0 [km]	Δy_0 [km]	Δz_0 [km]	Δt_0 [h]	z_0 [km]	σ_0(noise) [hPa] or [°C]
p	0.5	200	200	1	6	3	0.5
T	0.7	200	200	1	6	3	0.5
e	0.6	50	50	0.2	2	4	0.5

Table 2. Correlation parameters and variances used to interpolate path delays with COITROPA. The parameters apply to a GPS network density of around 10 stations per $100 \cdot 100$ km^2 and path delay intervals of 1–2 hr. Abbreviations: σ_0: *a priori* standard deviation of the signal; Δx_0, Δy_0, Δz_0, Δt_0: correlation lengths of the individual components; σ_0(noise): formal error of the GPS-derived path delay.

σ_0 [m]	Δx_0 [km]	Δy_0 [km]	Δz_0 [km]	Δt_0 [h]	σ_0(noise) [m]
0.01	100	100	1	6	[1)]

[1)] The σ_0(noise) is given by the GPS processing.

The mean rms of all profiles (Fig. 9) was compared to the *a posteriori* standard deviation of unit weight (Fig. 7). The strongest correlation is obtained with the solution AWATOS correlation ($R^2 = 0.27$). Only a slight correlation was achieved with the solution AWATOS AGNES ($R^2 = 0.10$). Considering this fact, it is assumed that the outliers on November 3, 6 and 9 on both types of data are caused by the meteorological variation in the troposphere during that period.

To quantify the accuracy of the profiles at different locations, the mean of the profile rms for all time points was determined. Fig. 10 shows a contour map of the mean rms of each profile compared to the aLMo data. Obviously, the highest rms is present for the northwestern most profiles. For the solution AWATOS correlation, the accuracy is varying in Switzerland whereas it is approximately constant for the solution AWATOS ANETZ. The COMEDIE solution behaves completely different. The rms is dependent on the number of ANETZ stations in the profile area.

5 CONCLUSION

This contribution deals with the determination of water vapour using a CGPS network geometry as it is available in Switzerland. Accurate GPS-derived path delays are obtained from the Swiss AGNES network. The delays are determined to correct for the tropospheric effect on GPS measurements as well as to derive the integrated amount of water vapour in the troposphere. To account for zenith path delays between the GPS stations, the use of the software package COITROPA has turned out to be feasible. In the case of lack of GPS data, reasonable accurate zenith path delays can be obtained by using meteorological data. The application of aLMo data provides a higher precision than the COMEDIE method, however, the latter is much less complex. The study revealed that both COITROPA and aLMo provide zenith wet path delays that fit better than 1 cm with the GPS-derived values.

A major challenge is to determine the spatial and temporal variation of water vapour. GPS-derived vertical profiles of water vapour in a high spatial and temporal resolution are obtained by applying a tomographic approach. This method has been successfully performed with the CGPS network AGNES. An analysis of the network design allows us to check the suitability of the GPS network and the geometry of the satellite's constellation. Furthermore, the influence of constraints is investigated. The use of *a priori* refractivity and intervoxel constraints is reasonable for the area of Switzerland. It is shown that the precision increases with the amount of voxels coupled with an *a priori* refractivity. A total of 6720 GPS-determined vertical refractivity profiles have been compared with data of the numerical weather model aLMo. An rms of around 5–8 ppm (refractivity unit) was achieved.

The results have shown that the CGPS network AGNES provides valuable information for research in atmospheric and meteorological sciences. Long-term time-series of the total amount of water vapour with high spatial and temporal resolution can be provided at relatively low cost. Moreover, the vertical resolution of water vapour allows numerous additional insights, such as into global and regional airflow and chemical processes in the atmosphere. GPS tomography has the potential to provide this data in 3-D spatial and high temporal resolution.

The launch of the European satellite navigation system GALILEO will roughly double the amount of satellites. It's impact on the tomographic technique remains to be investigated, but it can be assumed that the precision will further increase. Further research will focus on the improvement of the GPS-determined profiles and their reliability. The introduction of data of independent measurement sensors such as radiometers or spectrometers will be considered for improving the solution of the observation equations.

ACKNOWLEDGMENTS

We are grateful to Prof Dr M. Cocard, University Laval, Canada who supported this work by programming core routines of AWATOS and COMEDIE. Meteorological ground data are provided from the ANETZ of MeteoSwiss, and radiosonde data from the British Atmospheric Data Center. We thank Dr J.-M. Bettems of MeteoSwiss who enabled the comparison with data of the numerical weather model aLMo. Prof Dr M. Rothacher, GeoForschungsZentrum Potsdam, made helpful suggestions for the improvement of the paper. We are also grateful to two anonymous reviewers for critical comments and valuable advice. This research has been funded by the ETH Zürich and the Swiss Geodetic Commission of the Swiss Academy of Sciences.

REFERENCES

Beutler, G. *et al.*, 2001. Bernese GPS software version 4.2, eds Hugentobler, U., Schaer, S. & Fridez, P., Astronomical Institute, University of Berne, Switzerland.

Bevis, M., Businger, S., Herring, T., Rocken, C., Anthes, R. & Ware, R., 1992. GPS meteorology: Remote sensing of atmospheric water vapor using the global positioning system, *J. geophys. Res.,* **97**(D14), 15 787–15 801.

Brockmann, E. & Troller, M., 2002. GPS meteorology in the swiss alps: Interpolation accuracy for different alpine areas and near real-time results, In *Exploitation of Ground-Based GPS for Meteorology, COST Action 716 Workshop, GeoForschungsZentrum Potsdam, January 28–29*.

Doms, G. & Schättler, U. (eds.), 2003. Newsletter No. 3, February 2003. Technical Report, COSMO (Consortium for Small-Scale Modelling).

Essen, L. & Froome, K., 1951. The refractive indices and dielectric constants of air and its principal constituents at 24,000 mc/s. *Proceedings of the Royal Society B,* **64,** 862–875.

Kruse, L.-P., 2001. Spatial and temporal distribution of atmospheric water vapor using space geodetic techniques, *Geodätisch-geophysikalische Arbeiten in der Schweiz*, Vol. 61, Schweizerische Geodätische Kommission.

Mendes, V.B., 1999. Modeling the neutral-atmosphere propagation delay in radiometric space techniques, *PhD dissertation*, University of New Brunswick, Fredericton, New Brunswick, Canada.

Menke, W., 1989. *Geophysical Data Analysis: Discrete Inverse Theory,* Vol. 45 of International Geophysics Series, Academic Press, San Diego, CA, USA.

Moritz, H., 1973. Least-Squares Collocation, *PhD thesis*, DGK, Bayrische Akademie der Wissenschaften. Reihe AA: Theoretische Geodäsie, Heft Nr. 75.

Press, W., Teukolsky, S., Vetterling, W. & Flannery, B., 1994. *Numerical Recipes in C,* Cambridge University Press, Cambridge, UK.

Saastamoinen, J., 1972. Atmospheric correction for the troposphere and stratosphere in radio ranging of satellites, in *The use of artificial satellites for geodesy,* Vol. 15, pp. 247–251, eds Henriksen, S.W., Mancini, A. & Chovitz, B.H., Geophys. Monogr. Ser., AGU.

Troller, M., 2004. GPS based Determination of the Integrated and Spatially Distributed Water Vapor in the Troposphere. Diss. ETH No. 15513, ETH Zurich, Switzerland.

Troller, M., Cocard, M. & Geiger, A., 2000. Modellierung 4 dimensionaler Refraktionsfelder zur Berechnung von Weglängen-Korrekturen bei Satellitenmessungen. In *Simulation raumbezogener Prozesse: Methoden und Anwendungen,* Vol. 9, pp. 21–31, eds, Bernhard, L. & Krüger, T., IFGI prints, Institut für Geoinformatik, Westfälische Wiltrelms-Universität Münster, Germany.

Troller, M., Bürki, B., Cocard, M., Geiger, A. & Kahle, H.-G., 2002. 3d refractivity field from GPS double difference tomography, *Geophys. Res. Let.,* **29**(24), 2149–2152.

APPENDIX A: METEOROLOGICAL PATH DELAY MODELLING USING COMEDIE

COMEDIE allows a 4-D modelling of the meteorological parameters air pressure p, temperature T and water vapour pressure e in space and time. It is based on the method of least-squares collocation (Moritz 1973), that is, the model is described by a functional and a stochastic part. The functional models are selected based on approximated physical reality. Exponential functions are chosen for air pressure and water vapour pressure. Linear segments are used for the temperature:

$$p(x, y, z, t) = (p_0 + a(x - x_0) + b(y - y_0) + c(t - t_0)) \cdot \exp\left(-\frac{z - z_0}{H}\right), \tag{A1}$$

$$e(x, y, z, t) = (e_0 + a(x - x_0) + b(y - y_0) + c(t - t_0)) \cdot \exp\left(-\frac{z - z_0}{H}\right), \tag{A2}$$

$$T(x, y, z, t) = (T_0 + \gamma z) \cdot (1 - S(z - z_{\text{Tropopause}})) + a(x - x_0) + b(y - y_0) + c(t - t_0) + T_1 \cdot S(z - z_{\text{Tropopause}}) \tag{A3}$$

where:

$$S(z - z_{\text{Tropopause}}) = \frac{1}{\pi}\left[\arctan\left(\frac{z - z_{\text{Tropopause}}}{w}\right)\right] + 0.5$$

$S(z - z_{\text{Tropopause}})$ is used as a differentiable approximation of the Heavyside function with a step width w (unit: m). The observations are represented by the left-hand sides of eqs (A1)–(A3)

$p(x, y, z, t)$: air pressure at point $P(x, y, z)$ at time t
$e(x, y, z, t)$: water vapour pressure at point $P(x, y, z)$ at time t
$T(x, y, z, t)$: temperature at point $P(x, y, z)$ at time t

whereas the model parameters are being estimated (on the right-hand sides of eqs (A1)–(A3)):

p_0 : pressure at reference point $P_0(x_0, y_0, z_0)$ at time t_0
e_0 : water vapour pressure at reference point $P_0(x_0, y_0, z_0)$ at time t_0
T_0 : temperature at reference point $P_0(x_0, y_0, z_0)$ at time t_0
$z_{\text{Tropopause}}$: height of the tropopause
a, b, c : coefficients of the horizontal and temporal gradients
H : scale height
γ : temperature gradient with height
T_1 : temperature above the tropopause up to 20 km altitude

The reference coordinates x_0, y_0 and t_0 are calculated as means of all measurement points and times, except the height which is set to $z_0 = 0$.

The part not represented by the functional model, will be assigned to the stochastic model. It is decomposed into a signal and noise according to the covariance function, which describes the weighting of the individual sampling points to each other. In the present case, an anisotropic function has to be chosen to account for the topography. Furthermore, a damping factor is assigned to balance the high density of meteorological measurements on ground and the poor density in the higher atmosphere:

$$\Phi_{i,j} = \frac{\sigma_0^2}{1 + \left(\left(\frac{x_i - x_j}{\Delta x_0}\right)^2 + \left(\frac{y_i - y_j}{\Delta y_0}\right)^2 + \left(\frac{z_i - z_j}{\Delta z_0}\right)^2 + \left(\frac{t_i - t_j}{\Delta t_0}\right)^2\right) \cdot \exp\left(-\frac{z_i + z_j}{2z_0}\right)}, \tag{A4}$$

where:

$\Phi_{i,j}$: covariance function
σ_0^2 : a priori variance of the signal
$\overrightarrow{x_i} = \begin{pmatrix} x_i \\ y_i \\ z_i \\ t_i \end{pmatrix}, \overrightarrow{x_j} = \begin{pmatrix} x_j \\ y_j \\ z_j \\ t_j \end{pmatrix}$: space and time vector of point i and j
$\Delta x_0, \Delta y_0, \Delta z_0, \Delta t_0$: correlation length of the individual components
z_0 : scaling height

In Table 1, a set of correlation lengths and variances is presented, which are optimal for the subsequent investigations in Switzerland.

The collocation method allows to interpolate each meteorological parameter individually, both, in space and time. Using the formula of Essen & Froome (1951), the wet refractivity throughout the atmosphere can be determined. Finally, the refractivity is integrated along a ray in zenith direction to get the corresponding path delay.

APPENDIX B: MODELLING OF GPS-DETERMINED PATH DELAYS

COITROPA uses GPS-determined zenith path delays along with the associated 3-D coordinates and the time information. A least-squares collocation adjustment and interpolation is done similarly to COMEDIE. An exponential function is chosen as functional model:

$$\Delta^{PD}(x, y, z, t) = \left(\Delta_0^{PD} + a(x - x_0) + b(y - y_0) + c(t - t_0)\right) \cdot \exp\left(-\frac{z - z_0}{H}\right). \tag{B1}$$

The observation on the left-hand side of eq. (B1) is

$\Delta^{PD}(x, y, z, t)$: zenith path delay at point $P(x, y, z)$ at time t

whereas the model parameters are being estimated (on the right-hand side of eq. (B1)):

Δ_0^{PD} : zenith path delay at reference point $P_0(x_0, y_0, z_0)$ at time t_0
a, b, c : coefficients for the horizontal and temporal gradients
H : scale height

The reference coordinates (x_0, y_0) and the reference time t_0 are calculated as mean of all measurement points and times, except the height which is set to $z_0 = 0$.

The covariance function for the stochastic modelling corresponds to the implementation in COMEDIE (A4), however, the damping factor is omitted because of the lack of measurements in the higher atmospheric layers. Dedicated correlation lengths and variances for the AGNES network are given in Table 2.

APPENDIX C: APPROACH OF DOUBLE-DIFFERENCE PATH DELAYS

The GPS data are processed using the Bernese GPS Software (Beutler *et al.* 2001). For the steps that follow, the GPS-estimated zenith path delays as well as the double-difference residuals are required. Furthermore, the information about which stations and satellites are used to compose the double-differences must be available together with their respective time information.

First, the dry part of the zenith path delay has to be subtracted. The standard approach is to use some meteorological ground data of air pressure, temperature and water vapour pressure. They can be interpolated to the location of the GPS stations. Subsequently, using the formula of Saastamoinen (1972), the dry zenith path delay can be computed with sufficient accuracy.

The total GPS-estimated zenith path delay is reduced by the corresponding dry delay to obtain the zenith wet delay $\overline{\Delta^{PD}_{\mathrm{wet},p}}$ of station p. The latter is mapped to the respective elevation angle el^r_p (station p to satellite r) applying the same mapping function $m(el^r_p)$ as used in the GPS processing. The double-difference $\overline{\Delta^{2,PD,rs}_{\mathrm{wet},pq}}$ of the slant wet delays can now be formed (stations p,q, satellites r,s). Finally, the double-difference phase residual $\Delta^2\,\Phi^{rs}_{pq}$ is added. The following equation describes the reconstruction of the double-difference wet path delay $\Delta^{2,PD,rs}_{\mathrm{wet},pq}$:

$$\begin{aligned}\Delta^{2,PD,rs}_{\mathrm{wet},pq} &= \left(\Delta^{PD,r}_{\mathrm{wet},q} - \Delta^{PD,r}_{\mathrm{wet},p}\right) - \left(\Delta^{PD,s}_{\mathrm{wet},q} - \Delta^{PD,s}_{\mathrm{wet},p}\right)\\ &= \overline{\Delta^{2,PD,rs}_{\mathrm{wet},pq}} + \Delta^2\Phi^{rs}_{pq}\end{aligned} \tag{C1}$$

where:

$$\begin{aligned}\overline{\Delta^{2,PD,rs}_{\mathrm{wet},pq}} &= \left(\overline{\Delta^{PD}_{\mathrm{wet},q}}\cdot m(el^r_q) - \overline{\Delta^{PD}_{\mathrm{wet},p}}\cdot m(el^r_p)\right)\\ &\quad - \left(\overline{\Delta^{PD}_{\mathrm{wet},q}}\cdot m(el^s_q) - \overline{\Delta^{PD}_{\mathrm{wet},p}}\cdot m(el^s_p)\right)\end{aligned} \tag{C2}$$

APPENDIX D: USE OF INTERVOXEL CONSTRAINTS

The intervoxel constraints limit the variation of the difference in the refractivity of neighbouring voxels. As a result, underdetermined voxels are constrained to the mean of the neighbourhood and the refractivity at neighbouring voxels may be smoothed. To reduce the smoothing effect, only the direct neighbouring voxels in each dimension are taken into account. The weighting of the individual neighbouring voxels is derived from the following covariance function $\Phi_{i,j}$ which is dependent on the distance:

$$\Phi_{i,j} = \frac{\sigma_0^2}{1+\left[\left(\frac{x_i-x_j}{\Delta x_0}\right)^2+\left(\frac{y_i-y_j}{\Delta y_0}\right)^2+\left(\frac{z_i-z_j}{\Delta z_0}\right)^2\right]}, \tag{D1}$$

where:

$$\begin{aligned}\sigma_0^2 &: \textit{a priori}\text{ variance of the signal}\\ \vec{x_i} = \begin{pmatrix}x_i\\y_i\\z_i\end{pmatrix}, \vec{x_j} = \begin{pmatrix}x_j\\y_j\\z_j\end{pmatrix} &: \text{space vector of voxel centres } i \text{ and } j\\ \Delta x_0, \Delta y_0, \Delta z_0 &: \text{correlation lengths of the individual components}\end{aligned} \tag{D2}$$

Finally, for each voxel, a pseudo-observation equation is introduced in the tomographic equation system. Furthermore, for each pseudo-observation, a weight (regularization factor) with respect to the GPS double-difference observation has to be introduced in the covariance matrix of the equation system.